10

Discussion on Robust Control Applied to Active Magnetic Bearing Rotor System

Rafal P. Jastrzebski[1], Alexander Smirnov[1], Olli Pyrhönen[1]
and Adam K. Piłat[2]
[1]*Dept. of Electrical Engineering, LUT Energy, Lappeenranta University of Technology*
[2]*Dept. of Automatics, AGH University of Science and Technology, Krakow*
[1]*Finland*
[2]*Poland*

1. Introduction

Since the 1980s, a stream of papers has appeared on system uncertainties and robust control. The robust control relies on $\mathcal{H}_\infty$ control and μ synthesis rather than previously favored linear-quadratic Gaussian control. However, highly mathematical techniques have been difficult to apply without dedicated tools. The new methods have been consolidated in the practical applications with the appearance of software toolboxes, such as Robust Control Toolbox from Matlab. This chapter focuses on the application of this toolbox to the active magnetic bearing (AMB) suspension system for high-speed rotors.

AMBs are employed in high-speed rotating machines such as turbo compressors, flywheels, machine tools, molecular pumps, and others (Schweitzer & Maslen, 2009). The support of rotors using an active magnetic field instead of mechanical forces of the fluid film, contact rolling element, or ball bearings enables high-speed operation and lower friction losses. Other major advantages of AMBs include no lubrication, long life, programmable stiffness and damping, built-in monitoring and diagnostics, and availability of automatic balancing. However, AMB rotor system forms an open-loop unstable, multiple-input multiple-output (MIMO) coupled plant with uncertain dynamics that can change over time and that can vary significantly at different rotational speeds. In practical systems, the sensors are not collocated with the actuators, and therefore, the plant cannot always be easily decoupled. Additionally, the control systems face a plethora of external disturbances.

The major drawback of an AMB technology is a difficulty in designing a high-performance reliable control and its implementation. For such systems, the μ and $\mathcal{H}_\infty$ control approaches offer useful tools for designing a robust control (Moser, 1993; Zhou et al., 1996).

The high-performance and high-precision control for the nominal plant without uncertainties can be realized by using model-based, high-order controllers. In the case of control synthesis, which is based on the uncertain plant model, there is a tradeoff between the nominal performance (time- and frequency-domain specifications) and the robustness. The modeled uncertainties cannot be too conservative or otherwise obtaining practical controllers might be not feasible (Sawicki & Maslen, 2008). Moreover, too complex uncertainty models lead to increased numerical complexity in the control synthesis. The models applied for the control

synthesis of AMBs can vary from a point mass (Oliveira et al., 2006) to very complex MIMO plants (Li, Lin, Allaire & Luo, 2006).
The literature presents different weighting or interconnection design schemes. Each of the schemes has its contradictive objectives and tradeoffs. For the point mass levitated systems, the load uncertainty is typically applied. As an example, Li, Lin, Allaire & Luo (2006) present an **S**/**T**/**KS** scheme, where the **S**, **T**, **K**, and **G** are the sensitivity, complementary sensitivity, controller, and plant transfer functions. The corresponding weights are tuned using engineering judgment and manual trial and error simulations. Losch (2002) splits the available design schemes to signal-based and the loop-shaping schemes. The signal-based schemes are considered to be more complex and conservative. The loop-shaping schemes, for example, discussed by Losch (2002) include **KS**/**SG**/**T** for the control of the rigid rotor and **KS**/**SG**/**T**/**S** for the control of the flexible rotor. Another loop-shaping procedure is developed by Glover & McFarlane (1989). It applies robust stabilization of normalized coprime factorization of the plant using two weights: pre- and post-compensators. Skogestad & Postlethwaite (2005) give a general recommendation on the selection of these weights.
This chapter reviews different weighting schemes for building the robust control of AMB systems. The presentation starts with the point mass levitation and then undertakes non-gyroscopic and gyroscopic coupled AMB rotor systems. The aim of the robust control is to stabilize the rotor suspension independently to the assumed uncertainties. The robustness must be satisfied in the full range of the operating frequencies and for the selected range of the state variables. The work studies how to select the optimal control weighting functions for selected schemes based on genetic algorithms and experimental data obtained from the test rig. The Linear Parameter-Varying (LPV) technique is applied to suppress the influence of the variable rotational speed on the plant dynamics, thus reducing the uncertainty set. The real-time controller operating conditions are considered. The nonlinear simulations of the synthesized controllers and the accurate plant models in Simulink are compared with experimental results.

2. Suspension of the point mass

2.1 Introduction

The main component of the AMB system is an electromagnet that is used for the levitation purposes to keep the ferromagnetic object (e.g. rotor) levitated. The electromagnetic force value is controlled by the coil current steered by the external regulator. The introduction to the robust control is described by the example of Active Magnetic Suspension (AMS), which is also referred as Active Magnetic Levitation (AML). The robust approach can be applied to the uncertainty of the electromagnetic actuator and the levitated object mass. The controller synthesis and experiments are devoted to the MLS2EM (InTeCo, 2008) system (see Fig. 1) that extends the standard single electromagnet AML and represents one axis of the typical four horse-shoe AMB configuration.

2.2 Why robust control is required

In the classical state-feedback control approach for locally linearized AML model (Pilat, 2002) the mass uncertainty affects the control quality and object position. For the designed state-feedback controller with different closed-loop properties the 90 % mass perturbation has been introduced and presented with Bode diagrams in Fig. 2. One can find the influence of the mass change on the phase and amplitude depending on the designed controller properties.

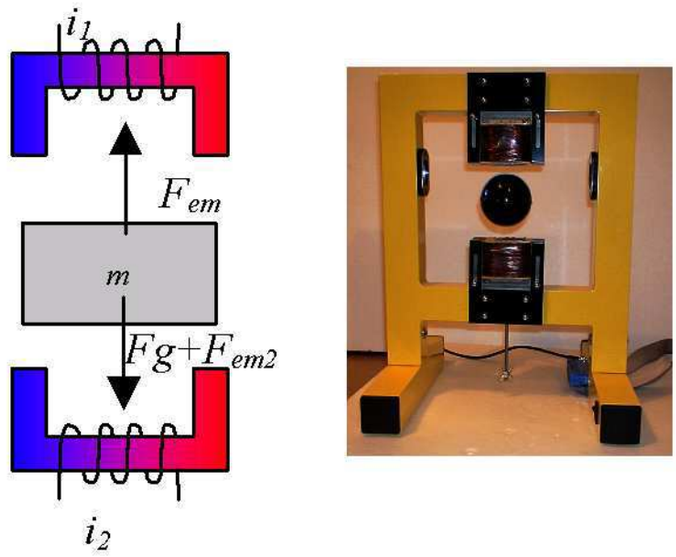

Fig. 1. Dual electromagnet Active Magnetic Levitation System - concept and test-rig.

The closed-loop characteristics remain unchanged due to the fixed and non-robust structure of the controller.

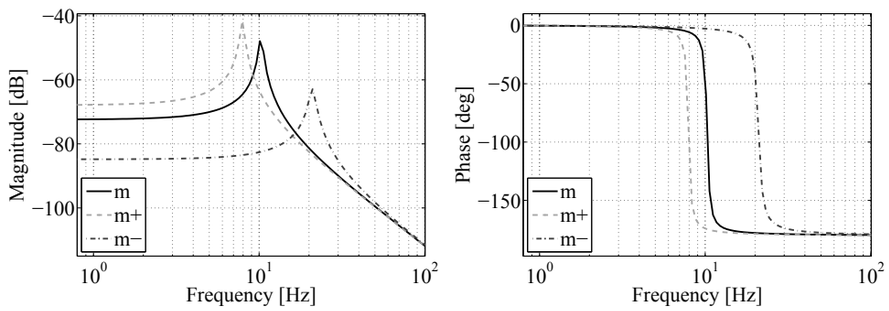

(a)

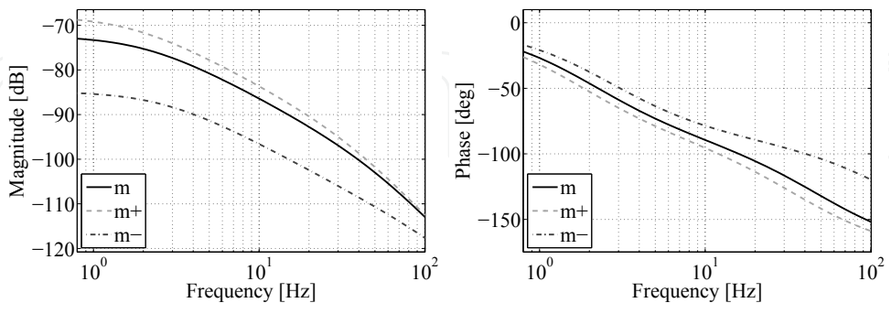

(b)

Fig. 2. Influence on the mass perturbation for the state feedback controller: a) for k = 250 $\mathrm{N\,m^{-1}}$, c = 0.2 $\mathrm{N\,s\,m^{-1}}$, b) for for k = 250 $\mathrm{N\,m^{-1}}$, c = 20 $\mathrm{N\,s\,m^{-1}}$.

The robust controller can be realized in the intelligent form by the application of the Fuzzy-Logic approach (Pilat & Turnau, 2005), where the controller is pre-tuned and optimized

at the modelling and simulation stage, or by the application of an on-line adopted neural network (Pilat & Turnau, 2009), where the weights and biases are updated while the real-time control is pending. Another approach is based on the linear control theory and parameter uncertainty. Some applications to the magnetic levitation and bearing systems can be found in (Fujita et al., 1995; Gosiewski & Mystkowski, 2008; Mystkowski & Gosiewski, 2009). The following section will present a robust controller design to stabilize the levitated object independently to its mass uncertainty. More detailed, simulation results and comparison to the state feedback controller can be found in (Pilat, 2010).

2.3 AML modelling and control

2.3.1 Nonlinear and linear AML model

The open loop structurally unstable model of the current driven single electromagnet AML (Pilat, 2009) is given by Equation (1).

$$\ddot{x_1} = -K_{\mathrm{em}} \frac{(i_0 + i)^2}{m(x_{10} + x_1)^2} + g, \tag{1}$$

where: x_1 - object displacement with respect to the x_{10} [m], x_{10} - nominal object distance from the electromagnet surface [m] (x_1>0), x_2 - object velocity [$\mathrm{m\,s^{-1}}$], m - object mass [kg], g - gravity acceleration [$\mathrm{m\,s^{-2}}$], K_{em} - actuator constant describing its construction [$\mathrm{N\,m^2\,A^{-2}}$], i - coil current [A], i_0 nominal coil current for the object distance x_{10}. This research will use the laboratory setup (Fig. 1b) characterized by the following parameter values: m = 0.056 kg, K_{em} = $5.594 \cdot 10^{-5}$ $\mathrm{N\,m^2\,A^{-2}}$. By analyzing the nonlinear model one can observe that the variable mass affects the system dynamics so that heavier objects require an increase in the coil current when the actuator construction remains the same. It means that the controller should react to the variable load using the robustness property. The steady-state coil current depends on the nominal object distance and the levitated object mass and the actuator design 2.

$$i_0(x_{10}, m) = x_{10} \sqrt{mgK_{\mathrm{em}}^{-1}}. \tag{2}$$

One can notice that the mass variation with respect to the nominal object mass is a source of demand for the coil current change. This should be satisfied automatically by the controller. To perform the controller synthesis for a chosen object position a linear model is required. The nonlinear model is linearized in the steady-state point $\boldsymbol{x}_0 = [0\ 0]^T$ resulting in the linear model in the form $\dot{\boldsymbol{x}} = \mathbf{A}\boldsymbol{x} + \mathbf{B}\boldsymbol{u}$, where:

$$\mathbf{A} = \begin{bmatrix} 0 & 1 \\ m^{-1}\alpha_0 & 0 \end{bmatrix}, \quad \mathbf{B} = \begin{bmatrix} 0 \\ m^{-1}\beta_0 \end{bmatrix} \tag{3}$$

with: $\alpha_0 = 2K_{\mathrm{em}} i_0^2 x_{10}^{-3}$ $\mathrm{kg\,s^{-2}}$, $\beta_0 = -2K_{\mathrm{em}} i_0 x_{10}^{-2}$ $\mathrm{kg\,m\,A^{-1}\,s^{-2}}$.

2.3.2 Robust controller design

The $\mathcal{H}_2$, $\mathcal{H}_\infty$ and μ-synthesis theory allows to perform an analysis and synthesis of the robust control systems (Battachatyya et al., 1995; Gu et al., 2005a; Kwakernaak, 1993; 2002) in the case of model-system uncertainties and perturbations. In the AML, the exact physical value of the levitated object mass is not known, but can be measured before an experiment. When applying the AML in real applications the mass value can vary. It can be assumed that the mass value is known with a certain, known interval. Thus, we can represent the mass as follows:

$$m = \overline{m}(1 + p_{\mathrm{m}}\delta_{\mathrm{m}}), \tag{4}$$

where $\overline{m}$ is the nominal value of m, and p_{m} and δ_{m} represent the relative perturbation on the object mass. The $\delta_{\mathrm{m}} \in [-1, 1]$ allows to perturb the mass vs. nominal value with a given ratio $p_{\mathrm{m}} \in [0, 1]$ corresponding to the percentage uncertainty. Let G_{ML0} denote the open-loop dynamics of the AMS taking into account the uncertainty of the levitated object mass. Thus, the AMS dynamics is given in the following form:

$$\begin{bmatrix} \dot{x}_1 \\ \dot{x}_2 \\ y_{\mathrm{m}} \\ y \end{bmatrix} = \mathbf{G}_{\mathrm{ML0}} \begin{bmatrix} x_1 \\ x_2 \\ u_{\mathrm{m}} \\ u \end{bmatrix}, \tag{5}$$

where:

$$\mathbf{G}_{\mathrm{ML0}} = \begin{bmatrix} \mathbf{A} & \mathbf{B}_1 & \mathbf{B}_2 \\ \mathbf{C}_1 & \mathbf{D}_1 & \mathbf{0} \\ \mathbf{C}_2 & \mathbf{D}_2 & \mathbf{0} \end{bmatrix}, \mathbf{A} = \begin{bmatrix} 0 & 1 \\ \overline{m}^{-1}\alpha_0 & 0 \end{bmatrix}, \mathbf{B}_1 = \begin{bmatrix} 0 \\ -p_{\mathrm{m}} \end{bmatrix}, \mathbf{B}_2 = \begin{bmatrix} 0 \\ \overline{m}^{-1}\beta_0 \end{bmatrix}, \tag{6}$$

$$\mathbf{C}_1 = \begin{bmatrix} \overline{m}^{-1}\alpha_0 & 0 \end{bmatrix}, \mathbf{C}_2 = \begin{bmatrix} 1 & 0 \end{bmatrix}, \mathbf{D}_1 = -p_{\mathrm{m}}, \mathbf{D}_2 = \overline{m}^{-1}\beta_0.$$

Note that the G_{ML0} depends only on the nominal AML parameters and the possible perturbation of a nominal object mass. The objective is to design the robust feedback controller $K(s)$ applied in the form:

$$u(s) = K(s)y(s). \tag{7}$$

The stability (8) of the nominal plant model as well as closed-loop robust stability (9) must be fulfilled.

$$\left\| \begin{bmatrix} W_p(1 + \mathbf{G}_{\mathrm{ML0}}K)^{-1} \\ W_u K(1 + \mathbf{G}_{\mathrm{ML0}}K)^{-1} \end{bmatrix} \right\|_\infty < 1 \tag{8}$$

$$\left\| \begin{bmatrix} W_p(1 + F_u(\mathbf{G}_{\mathrm{ML0}}, \delta_{\mathrm{m}})K)^{-1} \\ W_u K(1 + F_u(\mathbf{G}_{\mathrm{ML0}}, \delta_{\mathrm{m}})K)^{-1} \end{bmatrix} \right\|_\infty < 1 \tag{9}$$

The closed loop system with the designed controller, mass uncertainty and added weighting functions is presented in Fig. 3. The performance criterion is to have transfer functions from d to e_p and e_u small in the sense of $||\cdot||_\infty$ for all possible mass uncertainties. The weighting functions are used to reflect the relative significance of the performance requirement over different frequency ranges.

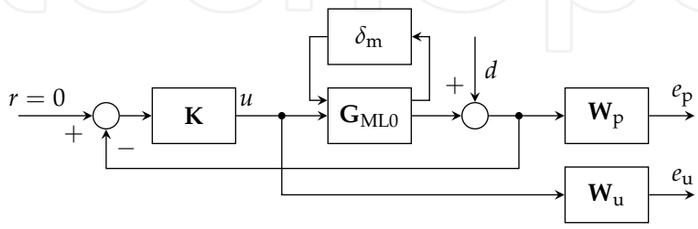

Fig. 3. AML closed loop system with an uncertain mass.

Thus, a key point in the controller design is to develop the sensitivity function to satisfy the required closed-loop performance over a specified frequency range. There are many possible approaches to propose the weighting functions, for example they can be chosen as follows:

$$W_p(s) = \frac{w_{\mathrm{n0}}}{w_{\mathrm{d1}}s + w_{\mathrm{d0}}}. \tag{10}$$

The control weighting function $W_u(s)$ is chosen as a scalar value of 10^{-3}. By adjusting the values of w_{n0}, w_{d1}, and w_{d0} the performance of the robust controller could be tuned up.
The robust μ-synthesis based on the D-K iteration procedure involving a set of optimizations produces the controller in a continuous form. The resulting controller order can be high and depend on the mass perturbation, formulation of the weighting function, and the number of iterations executed to find the optimal controller. The obtained 3^{rd} order controller has the following parameters: a_2=-1.473·10^6, a_1=-8.457·10^7, a_0 = -8.552·10^8, b_2 = 1.648·10^3, b_1 = 3.014·10^5, b_0 = 3.012·10^4 and it is given by equation (11).

$$K(s) = \frac{a_2s^2 + a_1s + a_0}{s^3 + b_2s^2 + b_1s + b_0}. \tag{11}$$

2.3.3 Real-time experiments

The realization of the AML controller is carried out using the MATLAB/Simulink and additional toolboxes. When steered from the PC-based platform, the I/O board is installed in the PC and RTW/RTWT toolboxes are applied to provide a real-time simulation in the Windows environment. When the control unit is based on the dSPACE controller and the Control Desk toolbox, the real-time controller is executed on the target embedded platform.
The dual electromagnet AML system driven by a frequency-based current hardware feedback controller was used to test the performance of the robust controller. The MLS2EM system was steered from the PC with a FastDAQ custom I/O board (Pilat & Piatek, 2008) from MATLAB/Simulink via RTWT at a sampling frequency of F_S = 4 kHz. The extra force generated in the programmable way and produced by the lower electromagnet was attracting the levitated object and therefore simulating mass uncertainty. To show the performance of the robust controller, the experimental data has been filtered to remove the high frequencies from the measured signals.
In the case of a step-type load representing a narrow mass change of 15 % the object is brought down to the desired level in 100 ms. The maximal overshoot versus desired object position is equal to 317 µm while for the triangular load corresponding to the low-frequency mass change of 33% is equal to 237 µm.

2.3.4 Conclusions to AML robust control design

The analytical robust control approach requires a good model of the system at the operating point. The parameter uncertainty does not cancel the structural nonlinearities, but is satisfactory for the required control performance. In some cases, the obtained high-order controller structure could not be realized by the hardware resources. In this case, the order reduction under special attendance of the controller quality is required.

3. Modelling of the AMB rotor systems

The second case study plant is a laboratory test stand with an AMB-supported custom rotor. The machine was originally a solid rotor induction motor for general industrial high-speed applications with the rated speed 12000 rpm. The original machine was produced by Rotatek Finland Oy. The AMB setup consist of two radial actuators and one axial actuator. The control

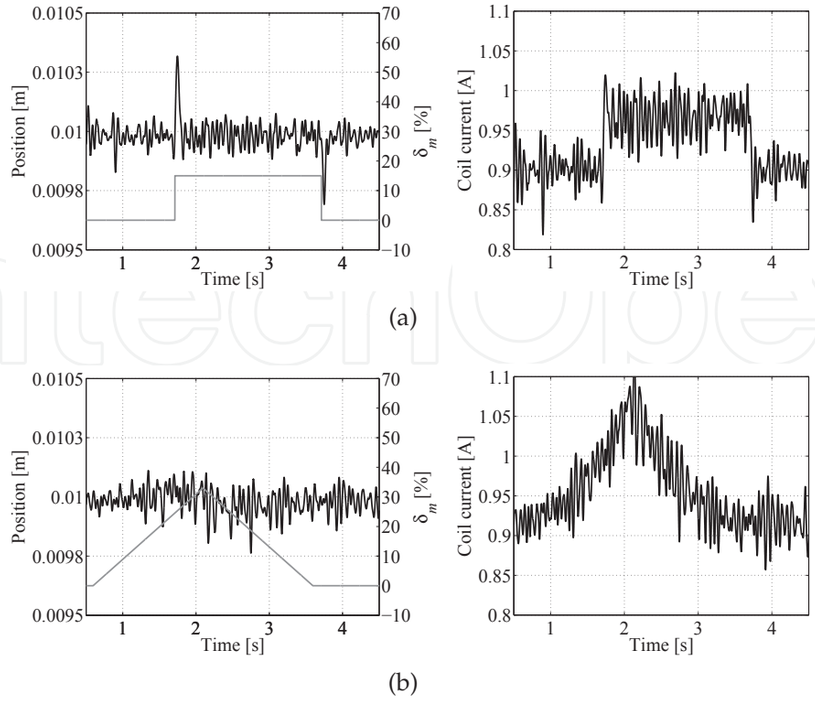

Fig. 4. Real-time experimens: a) narrow load change, b) slow load change.

layout comprises the inner current control loop and the outer position control loop. This section focuses on the radial suspension.

The studied AMB system is non-symmetric and non-collocated. The rotor is of a long rotor type without a significant gyroscopic effect. The machine is subcritical, that is, the maximum rotational speed is below the first flexible bending mode. From the radial position control point of view, the measured outputs are rotor displacements in two axes in two sensor planes and the applied control signals are four control currents of two radial eight-pole magnetic bearings. The system parameters are presented in Table 1.

Current stiffness and position stiffness	$k_i = 268\ \mathrm{N\,A^{-1}}$ and $k_x = 992\ \mathrm{N\,mm^{-1}}$
Rotor mass	46.2 kg
Rotor transverse moment of inertia	$4.8\ \mathrm{kg\,m^2}$
Rotor polar moment of inertia	$0.041\ \mathrm{kg\,m^2}$
Damping ratio of 1-3 flexible modes	0.0041, 0.0022, 0.0043
DC link voltage	150 V
Bias current and maximum currents	2.5 A and 10 A
Equivalent coil inductance and resistance	$L = 0.042$ H and $R = 0.43\ \Omega$
Equivalent average modulation delay	$\tau_{\mathrm{PWM}} = 25\ \mu\mathrm{s}$
Nominal magnetic air-gap lengths	0.6 mm

Table 1. Key AMB system parameters and their nominal values.

The technical details of the plant are given by Jastrzebski (2007), Jastrzebski & Pöllänen (2009) and Jastrzebski et al. (2010). The plant model comprises the actuator model and the rotor model.

3.1 Modelling of an AMB radial actuator

For each input-output channel, a complete nominal actuator model consists of a 2nd-order system with a pulse width modulation (PWM) delay and a motion-induced back electromotive force. The magnetic force relation for a single axis in each actuation plane in the close vicinity of the operating point is assumed to be

$$f = k_i i_\mathrm{c} + k_x x, \tag{12}$$

where k_i and k_x denote the current stiffness and the position stiffness. i_c and x are the control current and the position at the location of the bearings, respectively. Each of the inner current control loops is modeled as

$$\begin{bmatrix} \dot{i}_\mathrm{c} \\ \dot{u} \end{bmatrix} = \mathbf{A}_\mathrm{a} \cdot \begin{bmatrix} i_\mathrm{c} \\ u \end{bmatrix} + \mathbf{B}_\mathrm{ar}\dot{x} + \mathbf{B}_\mathrm{a} i_\mathrm{c,ref}, \quad i_\mathrm{c} = \mathbf{C}_\mathrm{a} \begin{bmatrix} i_\mathrm{c} \\ u \end{bmatrix}, \tag{13}$$

$$\mathbf{A}_\mathrm{a} = \begin{bmatrix} -\frac{R}{L} & \frac{1}{L} \\ -\frac{G_\mathrm{p}}{\tau_\mathrm{PWM}} & -\frac{1}{\tau_\mathrm{PWM}} \end{bmatrix}, \quad \mathbf{B}_\mathrm{ar} = \begin{bmatrix} -\frac{k_i}{L} \\ 0 \end{bmatrix}, \quad \mathbf{B}_\mathrm{a} = \begin{bmatrix} 0 \\ \frac{G_\mathrm{p}+G_\mathrm{ff}}{\tau_\mathrm{PWM}} \end{bmatrix}, \quad \mathbf{C}_\mathrm{a} = \begin{bmatrix} 1 \\ 0 \end{bmatrix}. \tag{14}$$

$i_\mathrm{c,ref}$ is the reference control current provided by the position control loop. G_p and G_ff are the proportional and feed-forward gains of the inner controllers.

3.2 Modeling of a mechanical subsystem

The rotor is modeled using a finite element method (FEM) custom code (Jastrzebski, 2007). The FEM model has 32 nodes, which corresponds to 128 degrees of freedom. The FEM code model is tuned to better correlate with the results of an experimental modal analysis of the free-free rotor and the results of frequency responses of the AMB levitated rotor (Jastrzebski et al., 2010). It is sufficient to retain only few lowest frequency modes. We apply the reduced unsupported rotor model for the controller synthesis. The model retains three flexible bending modes calculated at standstill in each plane (in the xz and yz planes). The equation of motion for the rotor spinning with the rotational speed Ω in the modal coordinates is

$$\mathbf{M}^\mathrm{m}\ddot{\boldsymbol{\eta}}^\mathrm{m} + (\mathbf{D}^\mathrm{m} + \Omega\mathbf{G}^\mathrm{m})\,\dot{\boldsymbol{\eta}}^\mathrm{m} + \mathbf{K}^\mathrm{m}\boldsymbol{\eta}^\mathrm{m} = \boldsymbol{f}^\mathrm{m}. \tag{15}$$

The matrices of the mechanical system description $\mathbf{M}^\mathrm{m}$, $\mathbf{K}^\mathrm{m}$, $\mathbf{G}^\mathrm{m}$ and $\mathbf{D}^\mathrm{m}$ are the diagonal mass matrix, the diagonal stiffness matrix, the skew-symmetric gyroscopic matrix, and the damping matrix, respectively. $\boldsymbol{f}^\mathrm{m}$ and $\boldsymbol{\eta}^\mathrm{m}$ are the vector of the modal forces acting on the rotor and the vector of modal coordinates. In fact, the first four coordinates correspond to the rigid rotor modes in the center of gravity coordinates. This reduced rotor model has in total ten coordinates.

In order to include the bearing stiffness matrices $\mathbf{K}_i$ and $\mathbf{K}_x$ in the rotor model, a transformation $\mathbf{C}_\mathrm{f}$ from the position of actuators to the center of mass is applied. Additionally, the model has to provide rotor displacements in the position of sensors and velocities at the location of bearings. Thus, another transformation matrixes are necessary $\mathbf{C}_\mathrm{s}$ and $\mathbf{C}_\mathrm{b}$.

Finally, after removing the superscript 'm' for modal, the state space equations of the rotor-bearing system has the following form

$$\begin{aligned}
\mathbf{A}_\mathrm{r} &= \begin{bmatrix} \mathbf{0} & \mathbf{I} \\ -\mathbf{M}^{-1}\left(\mathbf{K} - \mathbf{C}_\mathrm{f}^T \mathbf{K}_x \mathbf{C}_\mathrm{f}\right) & -\mathbf{M}^{-1}\left(\mathbf{D} + \Omega\mathbf{G}\right) \end{bmatrix}, \\
\mathbf{B}_\mathrm{r} &= \begin{bmatrix} \mathbf{0} \\ -\mathbf{M}^{-1}\mathbf{C}_\mathrm{f}^T \mathbf{K}_i \end{bmatrix}, \\
\mathbf{C}_\mathrm{rs} &= \begin{bmatrix} \mathbf{C}_\mathrm{s} & \mathbf{0} \end{bmatrix}, \\
\mathbf{C}_\mathrm{rb} &= \begin{bmatrix} \mathbf{0} & \mathbf{C}_\mathrm{b}. \end{bmatrix}
\end{aligned} \tag{16}$$

3.3 Complete nominal plant model

The resulting equation for the full system, which combines the rotor and actuator has the following form

$$\mathbf{A} = \begin{bmatrix} \mathbf{A}_\mathrm{a} & \mathbf{B}_\mathrm{ar}\mathbf{C}_\mathrm{rb} \\ \mathbf{B}_\mathrm{r}\mathbf{C}_\mathrm{a} & \mathbf{A}_\mathrm{r} \end{bmatrix}, \quad \mathbf{B} = \begin{bmatrix} \mathbf{B}_\mathrm{a} \\ \mathbf{0} \end{bmatrix}, \quad \mathbf{C} = \begin{bmatrix} \mathbf{0} & \mathbf{C}_\mathrm{r} \end{bmatrix}. \tag{17}$$

The open-loop transfer function of the plant in the Laplace domain using the state variable form can be written as

$$\mathbf{y} = \mathbf{G}\left(s\right)\boldsymbol{u} = \mathbf{C}\left(s\mathbf{I} - \mathbf{A}\right)^{-1}\mathbf{B}\boldsymbol{u}. \tag{18}$$

$\mathbf{G}(s)$ is a transfer function matrix of the plant. $\boldsymbol{u}$ and $\boldsymbol{y}$ are the vectors of the control currents and the measured displacements, respectively. $\mathbf{A}$, $\mathbf{B}$, and $\mathbf{C}$ are the state matrix, the input matrix, and the output matrix in the state-space representation, respectively. The combined actuator and rotor models form a coupled plant, which has 28 states. The coupling between the transversal and tilting rotor movements is caused by the radial actuators. The coupling between the xz and yz planes appears as a result of the gyroscopic coupling (Jastrzebski, 2007). In order to decrease the condition number of the plant, the MIMO coupled plant model applies a similarity transformation leading to a normalized per-unit (pu) system. Such a per-unit plant is less prone to numerical problems when designing a controller.

3.4 Modeling of uncertainties

We divide uncertainties into dynamic perturbations and disturbance signals (Gu et al., 2005b). The disturbances originate from the inverter, motor and the load transmitted forces, as well as sensor and actuator noise. These disturbances are difficult to measure and model but some rough estimations can be applied. The dynamic perturbations comprise unstructured uncertainties, when the perturbations are only considered by upper and lower bounds, and the structured uncertainties when the perturbations appear in particular parameters (Skogestad & Postlethwaite, 2005). The former ones are unmodelled dynamics of the base and truncated high-frequency modes of the rotor. The letter ones are neglected nonlinearities of the actuators and sensors and other variations of nominal system parameters.
The structured uncertainties in the actuator include:

- variable current stiffness and position stiffness because of modeling inaccuracies, actuator nonlinearities, and changes of the operational point ($\pm$10 %)
- variation of electrical parameters of the actuator ($\pm$10 %)

The effects of hysteresis and time delays (of the modulation, digital control, and sensors) can be neglected for the applied system components.

The structured uncertainties when considering mechanical models and position sensors are:

- variable mass resulting from external low-frequency loads depending on applications, e.g., in compressors and pumps (± 10 %)
- variable sensor gain and offset (± 5 %)
- uncertain sensor locations (± 1 %)
- variation of the rotational speed
- uncertainties in the modal mass and damping matrices (± 2 %)

The uncertainty in the sensor locations emulates uncertainty of the mode shapes of the bearings, which are more difficult to implement. The most notable variations occur because of changes in the operational speed and shifting of the operational point. The shifting occurs for the nonzero reference position, in the presence of sensing errors, rotor runout, and external forces.

All or some of the dynamic perturbations can be lumped into a single perturbation block Δ. Δ is referred to as an unstructured uncertainty and it is complex whereas the parametric uncertainties are assumed to be real.

Differences between the measured frequency responses of the test-rig and the nominal plant model that are significant and otherwise not covered by the structured uncertainties (Jastrzebski et al., 2010) are modeled as an unstructured uncertainty. In particular, the structural resonance of the base of the machine at about 1130 rad/s (180 Hz), is modeled using an output multiplicative uncertainty $\mathbf{\Delta} = \mathbf{\Delta}_{\mathrm{o}}$.

The uncertain plant with a multiplicative output uncertainty in each input-output channel is

$$\mathbf{G}_{\mathrm{p}} = \left(\mathbf{I} + w_{\mathrm{o}}\mathbf{\Delta}_{\mathrm{o}}\right)\mathbf{G},\ \left\|\mathbf{\Delta}_{\mathrm{o}}\right\|_{\infty} \leq 1. \tag{19}$$

$w_{\mathrm{o}}(s)$ is an uncertainty scalar weight with appropriately selected coefficients a_i such as

$$\left|w_{\mathrm{o}}(j\omega)\right| \geq l_{\mathrm{o}}(\omega)\,\forall\omega,\ l_{\mathrm{o}}(\omega) = \max_{\bar{\sigma}}\left(\left(\mathbf{G}_{\mathrm{p}} - \mathbf{G}\right)\mathbf{G}^{-1}(j\omega)\right), \tag{20}$$

$$w_{\mathrm{o}}(j\omega) = \frac{a_0 s^2 + a_1 s + a_2 s^2}{s^2 + a_3 s + a_4 s^2}. \tag{21}$$

$\|.\|_{\infty}$ and $\bar{\sigma}$ denote the $\mathcal{H}_{\infty}$ norm and the maximum singular value (Skogestad & Postlethwaite, 2005), respectively. When the uncertain parts are separated from the dynamics, the system can be presented in a well-known upper linear fractional transformation (LFT) $F\left(\mathbf{M}, \mathbf{\Delta}\right)$, where $\mathbf{M}$ represents a standard interconnection of the system with uncertainties taken out. Now, $\mathbf{\Delta}$ consists of both the unstructured and parametric uncertainties. The uncertain block $\mathbf{\Delta}$ is a diagonal matrix.

The analysis and design are more difficult when the structural uncertainties are real numbers. Unfortunately, the use of the lumped full model also results in a pessimistic analysis and a conservative design (Gu et al., 2005b). Therefore, a proper selection of modeled uncertainties is not straightforward.

After analyzing the suspension of the point mass, which can be treated equivalently to the axial suspension of the rotor, we focus on the radial suspension.

4. $\mathcal{H}_\infty$ control of the AMB rotor system with insignificant gyroscopic effect

Different weighting schemes are applicable to form a cost function subject to the $\mathcal{H}_\infty$ norm in (sub)optimization problems. Perhaps the most commonly applied schemes are the $\mathbf{S/KS}$ and $\mathbf{S/T}$ schemes. The $\mathbf{S/KS}$ scheme can achieve nominal performance in tracking or disturbance rejection and robust stability against the additive perturbations. The weighted mixed sensitivity $\mathbf{S/T}$ scheme can achieve nominal performances and robust stability against multiplicative perturbations. However, in the aforementioned schemes there is a danger of pole-zero cancellation between the nominal model and the controller (Sefton & Glover, 1990). They are also limited by the condition of the number of the right-half plane poles. In the perturbed system the number should be the same as in the nominal one (Lunz, 1989). In response to these limitations, another weighting scheme features robust stabilization against normalized coprime factor perturbation of the nominal plant. The $\mathcal{H}_\infty$ loop-shaping design relaxes the right-half plane restrictions and produces no pole-zero cancellation. The solution is obtained directly without the need for iterations.

4.1 Loop-shaping Glover-McFarlane control of an AMB rotor system

A loop-shaping $\mathcal{H}_\infty$ design procedure was introduced by Glover & McFarlane (1989). Later, it was extended to the two-degrees of freedom problem by Limebeer et al. (1993). The approach gained its popularity as it does not require a γ-iteration and provides a result by solving two Riccati equations.

To achieve a controller based on a loop-shaping technique, two weights should be selected. This is a pre-compensator $\mathbf{W}_1$ and a post-compensator $\mathbf{W}_2$. They alter the open-loop transfer function of the plant $\mathbf{G}$ to the desired shape $\mathbf{G}_\mathrm{s}$. Selection of weights depends on the performance and robustness criteria. Additionally, weights can be selected based on the presented multiplicative uncertainties. Structured uncertainty is not supported directly by the method. In a case where there are many sources of uncertainties, other methods prove to be conservative or too difficult to apply. Hence, multiplicative uncertainty approximated on the representative set of plants is a useful solution.

After selecting weights and multiplying the nominal plant from left and right, the system is stabilized with an $\mathcal{H}_\infty$ controller $\mathbf{K}_\mathrm{s}$ see Fig. 5(a). The final controller $\mathbf{K}$ is obtained as

$$\mathbf{K} = \mathbf{W}_1\mathbf{K}_\mathrm{s}\mathbf{W}_2. \tag{22}$$

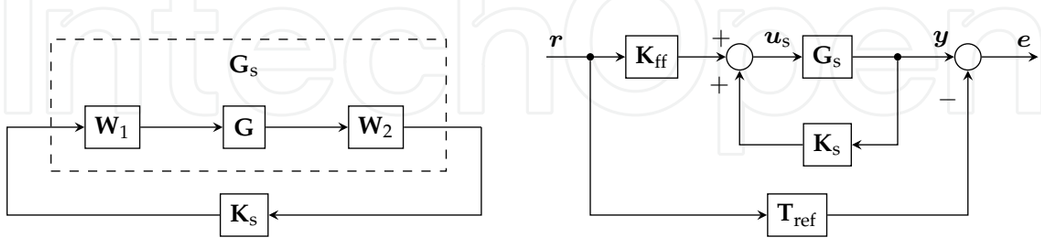

(a) Glover-McFarlane controller structure (b) Two degrees-of-freedom design problem

Fig. 5. Loop-shaping controllers

As a next step, a feedforward part is added. For that, a reference transfer function $\mathbf{T}_\mathrm{ref}$ should be chosen. The feedforward controller $\mathbf{K}_\mathrm{ff}$ is obtained by minimizing the following problem

$$\|(\mathbf{I} - \mathbf{G}_\mathrm{s}\mathbf{K}_\mathrm{s})^{-1}\mathbf{G}_\mathrm{s}\mathbf{K}_\mathrm{ff} - \mathbf{T}_\mathrm{ref}\|_\infty \leq \gamma \tag{23}$$

The described method is based mainly on the weight selection. The pre-compensator is usually a low-pass filter. Additional features can be included in the weight such as a notch filter, which is particularly useful in the described application to suppress the flexible modes. The post-compensator is used to emphasize one output over the other. As in the AMB system, all the outputs are equivalent, and this weight is a constant diagonal matrix. The last weight $\mathbf{T}_{\text{ref}}$ should describe the desired transfer function of a closed-loop plant. Thus, a first-order transfer function with a steady state gain equals one, and a crossover frequency is chosen to correspond to the desired bandwidth of the system.

This procedure for an AMB system was applied by Fujita et al. (1993), where the authors give a review how to choose weights based on the multiplicative uncertainties in the system. The applied model of the system was relatively simple accounting only for rigid modes. The loop-shaping method was combined with a μ-synthesis procedure by Lanzon & Tsiotras (2005) to guarantee performance specifications and tolerate structured uncertainties. The resulting controller was successfully applied to the AMB system.

In this work, for the controller synthesis, the procedure suggested by (Skogestad & Postlethwaite, 2005, ch. 9.4.2) is applied. The process is the same as described earlier with an addition of calculation gains to ensure the desired steady-state response. The reference function $\mathbf{T}_{\text{ref}}$ is chosen as

$$\mathbf{T}_{\text{ref}} = \mathbf{I}_{4\times 4}\frac{1}{\frac{1}{\omega_{\text{bw}}}s+1}, \tag{24}$$

where $\omega_{\text{bw}} = 215$ rad/sec is the bandwidth of the closed-loop system.

The pre-compensator transfer function is chosen to be a low-pass filter with a DC gain of 78.1 dB. Additionally, the weight includes a notch filter as a second-order transfer function. The damping frequency is $1.664 \cdot 10^3$ rad s^{-1} and the damping ration is 0.08. The final transfer function is as follows

$$\mathbf{W}_1 = \mathbf{I}_{4\times 4}\frac{s+110}{s+0.01365}\cdot\frac{\left(\frac{s}{1.664\cdot 10^3}\right)^2+\frac{0.3\cdot 0.08}{1.664\cdot 10^3}s+1}{\left(\frac{s}{1.664\cdot 10^3}\right)^2+\frac{0.3}{1.664\cdot 10^3}s+1}. \tag{25}$$

Using the weight (25) presented in Fig. 6(a) and the reference function (24), a two-degrees of freedom controller is synthesised. The order of the controller is reduced to fit the real-time implementation using a Schur method (Safonov & Chiang, 1988). The evaluation of the controller with a μ-analysis is presented in Fig. 6(b).

The plot shows that the controller is capable of handling the modeled structured uncertainty. All the values are below one. As it was expected, the highest values are spotted near the first flexible mode. However, the use of a notch filter helps to alleviate the problem. The experimental evaluation of the controller is discussed in section 4.6.

4.2 $\mathcal{H}_\infty$ signal-based control of an AMB rotor system

For the simple weighting schemes in the frequency domain, for example, such as the $\mathbf{S}/\mathbf{KS}$ mixed sensitivity problem, which provides good tracking and limits control energy, we are not able to include more complex specifications. The more versatile schemes are signal-based $\mathcal{H}_\infty$ approaches. However, the more complex the resulting lower LFT becomes, the more difficult the selection of the multiple design weights and the more complex and difficult the numerical solution of the minimization problem are. We modify the Skogestad & Postlethwaite (2005) scheme by lifting up the restrictions on all of the states but instead adding application-specific

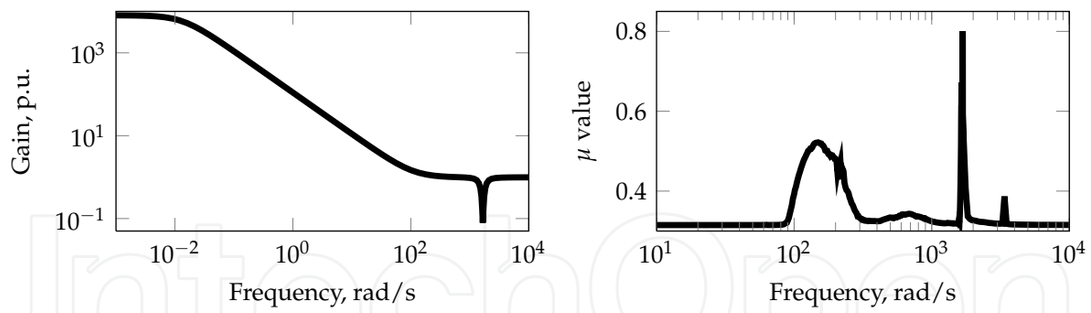

(a) Pre-compensator shape in the frequency domain

(b) μ-analysis

Fig. 6. $\mathcal{H}_\infty$ loop-shaping design

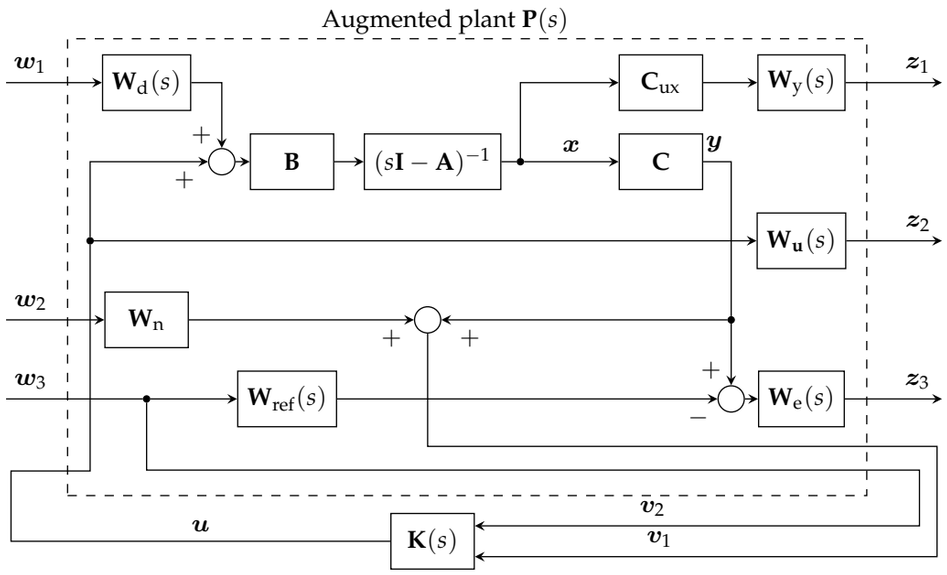

Fig. 7. 2DOF $\mathcal{H}_\infty$ signal-based design problem.

voltage limitation and displacement limitations at critical locations other than sensor planes. Now, a magnetic bearing system can be described using a general control configuration (Fig. 7). The stabilizing controller can be found by minimizing the $\mathcal{H}_\infty$ norm from the exogenous inputs $\boldsymbol{w} = [\boldsymbol{w}_1, \boldsymbol{w}_2, \boldsymbol{w}_3]^\mathrm{T}$ to the exogenous outputs $\boldsymbol{z} = [\boldsymbol{z}_1, \boldsymbol{z}_2, \boldsymbol{z}_3]^\mathrm{T}$. The inputs to the controller $\boldsymbol{v}_1$ and $\boldsymbol{v}_2$ are the vector of the position reference signals and the vector of the distorted signals received from the displacement sensors, respectively. The augmented plant input vectors $\boldsymbol{w}_1$, $\boldsymbol{w}_2$ and $\boldsymbol{w}_3$ are the vector of the input distortion signals, the vector of the output distortion signals, and the vector of the reference signals, respectively. The augmented plant output vectors $\boldsymbol{z}_1$, $\boldsymbol{z}_2$, and $\boldsymbol{z}_3$ are the vector of the voltages and displacements obtained using the output matrix $\mathbf{C}_{ux}$, weighted system input signals, and the vector of the weighted position error signals, respectively.

The signal limitations result in the unitary weight for the normalized plant special outputs $\mathbf{W}_y = \mathbf{I}$. The sensor noise spectrum is approximated by the first-order high-pass filter $\mathbf{W}_\mathrm{n}$ with the dc gain and the high-frequency gain equal to 0.2 % and 5 % of the measuring range. The crossover frequency is 250 Hz.

The weights $\mathbf{W}_{\mathrm{d}}(s)$, $\mathbf{W}_u(s)$, and $\mathbf{W}_e(s)$ are defined as first-order transfer functions multiplied by a 4×4 unitary matrices. The coefficients of these functions are treated as design parameters. Applying the $\mathcal{H}_\infty$ control problem, the admissible controller $\mathbf{K}$ is found, if one exists, so that for $\gamma > 0$

$$\|\mathbf{F}_{\mathrm{l}}(\mathbf{P},\mathbf{K})\|_\infty = \max_\omega \bar{\sigma}\left(\mathbf{F}_{\mathrm{l}}\left(\mathbf{P},\mathbf{K}\right)\left(j\omega\right)\right) \leq \gamma. \tag{26}$$

4.3 Control design specification

For all of the schemes, the appropriate choice of the weighting functions, which provide guaranteed stability, robustness margin, and tracking nominal performance, is required. The structure and order of the weights should deliver enough flexibility but without too much added complexity in the optimization. The order of the weights together with the order of the nominal plant decide if and how easily the satisfactory solution can be obtained using necessary numerical procedures.
When defining the control design specification the major points are:

- closed-loop stability
- limitations of actuators, i.e., maximum coil current and limited DC link voltage and as a result, limited force slue rate
- no steady-state error
- sufficient input disturbance rejection and noise rejection of the sensors (output)
- robust stability and robust performance
- minimization of the output sensitivity peak

Additionally, the minor objectives are: desired step responses and the closed-loop bandwidth within the desired range.
The most of the listed objectives are easily tested. However, in order to test robust stability, the structural singular value μ has to be computed (Gu et al., 2005b; Skogestad & Postlethwaite, 2005; Zhou, 1998)

$$\mu_\Delta^{-1}(\mathbf{M}) := \min_{\mathbf{\Delta}\in\mathbf{\Delta}_{\mathrm{s}}} \left\{\bar{\sigma}(\mathbf{\Delta}) : \det\left(\mathbf{I} - \mathbf{M}\mathbf{\Delta}\right) = 0\right\}. \tag{27}$$

$\mathbf{M}$ is the interconnected closed-loop system transfer function matrix and $\mathbf{\Delta} \in \mathbf{\Delta}_{\mathrm{s}}$ represents uncertainties. $\mathbf{M}(s)$ is formed with respect to the uncertainty set $\mathbf{\Delta}_{\mathrm{s}}$

$$\mathbf{\Delta}_{\mathrm{s}} = \left\{ \mathrm{d}iag\left[\delta_1 I_{1r}, \cdots, \delta_s I_{rs}, \Delta_1, \cdots, \Delta_f\right] : \delta_i \in C, \Delta_j \in C^{m_j \times m_j} \right\}, \tag{28}$$

where $\sum_{i=1}^{s} r_i + \sum_{j=1}^{f} m_j = n$ with $\mathbf{M} \in C^{n\times n}$. n equals to the dimension of the block $\mathbf{\Delta}$. s and f are the dimensions of the scalar and full uncertainty blocks, respectively.
The structural singular value of $\mathbf{M}(s)$ is a measure of the robust stability of the uncertain system

$$\mu_\Delta\left(\mathbf{M}(s)\right) := \sup_{\omega\in R} \mu_\Delta\left(\mathbf{M}(j\omega)\right). \tag{29}$$

For normalized uncertainties, the system in a standard configuration is robustly stable if $\mathbf{M}(s)$ is stable and $\mu_\Delta\left(\mathbf{M}(s)\right) < 1$. The robust performance requires that the closed-loop control system performs satisfactorily even in the presence of the defined plant uncertainties. The robust performance problem can be solved by generalizing to the robust stabilization problem

with the uncertainty block replaced by $\tilde{\mathbf{\Delta}} \in \tilde{\mathbf{\Delta}}_{\mathrm{s}} := \mathrm{diag}\left\{\mathbf{\Delta}, \mathbf{\Delta}_{\mathrm{p}}\right\}$, where the uncertainties are normalized and the fictious performance uncertainty block is bounded by the norm $\left\|\mathbf{\Delta}_{\mathrm{p}}\right\|_{\infty} \leq 1$. $\mathbf{\Delta}_{\mathrm{p}}$ is unstructured with appropriate dimensions defined by the exogenous inputs and error outputs of the system $\mathbf{M}$ to represent system performance specifications.

4.4 Weighting functions as design parameters

An elegant solution to alleviate the weight selection procedure is the μ-synthesis approach. For the system with a specified uncertainty set, the algorithm gives the weights that result in a robustly stable controller obtained by an $\mathcal{H}_{\infty}$ synthesis. The main drawback is that there is no analytical solution for the problem. The procedure is iterative and computationally expensive. It results in a controller of a very high order. What is more, the performance requirements are again specified as initial weights, and the designer should also choose a specific weighting scheme. Last but not least, the resulting order of the controller depends on the complexity of the applied weighting scheme, plant order, and applied uncertainties. Detailed interconnections lead to controllers, which are difficult to implement and are not transparent.

For complex systems, such as the flexible AMB rotor system, finding appropriate performance weights by trial and error is very time consuming. To find the weights that produce a design meeting the multiple requirements, we could use the optimization based on the method of inequalities (Whidborne et al., 1994) or the linear matrix inequalities (Scherer et al., 1997). Another option for such a multibjective design is to apply a basic genetic algorithm (GA) (Jastrzebski et al., 2010).

For a signal-based weighting scheme, the coefficients of the weights $\mathbf{W}_{\mathrm{d}}(s)$, $\mathbf{W}_{u}(s)$, and $\mathbf{W}_{e}(s)$ are limited by its minimum and maximum selected values because of numerical reasons. Also for numerical reasons and to prevent unwanted pole-zero cancellation (Gu et al., 2005b) the stable and minimum-phase weights are applied. For continuous-time weights in the Laplace domain both the zeros and poles of a minimum phase weight must be strictly inside the left-half s-plane.

4.5 Genetic algorithm approach to multiobjective synthesis

The $\mathcal{H}_{\infty}$ optimization and the μ-synthesis result in the complex controllers of the higher order than the plant. In an effort to obtain a lower-order controller, we could reduce the plant model by truncating the high-frequency modes beyond the actuator bandwidth prior to the controller synthesis. In the iterative design, the resulting lower-order controller could be tested in each iteration together with the higher-order non-reduced plant against the multi-objective performance function. An alternative procedure to obtain a lowest-order controller is to use the detailed plant model for the synthesis and to apply the controller-order reduction afterwards. Both approaches replace a direct design of the low-order controller.

For the signal-based weighting scheme, some of the signal weights are kept constant while the others, which are the free parameters in the optimizations, are varied in order to reach the optimal design in the multi-objective control design problem. The basic genetic algorithm search is improved by limiting the feasible solution space. This improves the numerical conditioning, and the weights without physical relevance are excluded from the solutions (Jastrzebski et al., 2010).

The design objectives are normalized by the desired limiting values and are proportional to the square of the following performance indices:

- Output sensitivity peak $M_S = \|\mathbf{S}_\mathrm{o}\|_\infty$ and the closed-loop bandwidth (the frequency where $\bar{\sigma}(\mathbf{S}_\mathrm{o})$ first crosses 0.7 from below.
- High controller gain (a small maximum singular value of the sensitivity) at low frequencies $\bar{\sigma}\left(\mathbf{S}_\mathrm{o}(\omega)\right)$, where $\omega \to 0$.
- Input disturbance attenuation $M_{T\mathrm{i}} = \left\| \mathbf{K}_\mathrm{fb}\mathbf{G}\mathbf{S}_\mathrm{i}\ \mathbf{G}\mathbf{S}_\mathrm{i} \right\|_\infty$ and output disturbance attenuation $M_{T\mathrm{o}} = \left\| \mathbf{G}\mathbf{K}_\mathrm{fb}\mathbf{S}_\mathrm{o}\ \mathbf{K}_\mathrm{fb}\mathbf{S}_\mathrm{o} \right\|_\infty$.
- Value of γ.

The norms $M_{T\mathrm{i}}$ and $M_{T\mathrm{o}}$ minimize the usage of control signals and the plant output signals in the presence of the input and output distortion signals, respectively. The sensitivity functions are defined as

$$\mathbf{S}_\mathrm{o} = (\mathbf{I} + \mathbf{G}\mathbf{K})^{-1}, \quad \mathbf{S}_\mathrm{i} = (\mathbf{I} + \mathbf{K}\mathbf{G})^{-1}. \tag{30}$$

After applying GA and obtaining a final $\mathcal{H}_\infty$ controller the closed-loop uncertain system is

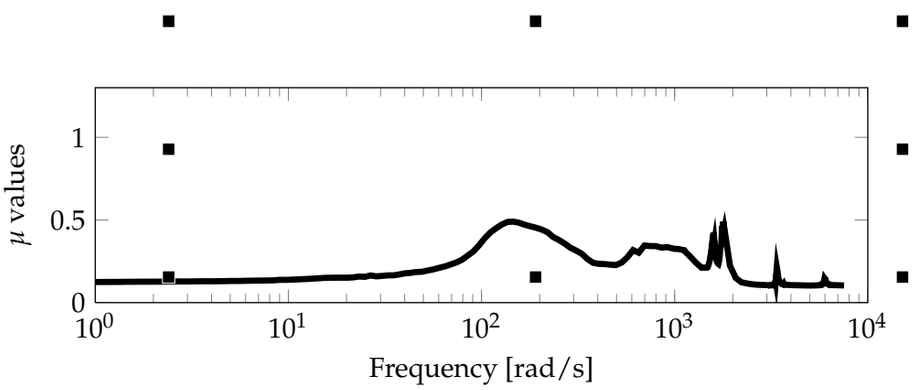

Fig. 8. μ analysis for robust stability.

tested for robust stability (Fig. 8) and performance. In order to limit design conservativeness in $\mathcal{H}_\infty$ control the uncertainties in the plant model, which is applied for design synthesis, are limited to the uncertain speed. In the case of the structured uncertainty, the computation of the structural singular value μ has to be applied and the μ synthesis remains an open problem. When applying the weights obtained using the GA to the μ synthesis, the μ synthesis cannot considerably improve the initial γ value.

4.6 Control validation

The controller achieved in section 4.1 is applied for radial AMBs in the test rig. First, the frequency responses are compared. The output sensitivity function for the B-end of the rotor is measured. The results are presented in Fig. 9. The theoretical values coincide the values obtained from the prototype. One peak that is not presented in the theoretical model corresponds to the natural frequency of the foundation. The foundations were not taken into account in the described synthesis method. Additionally, the values vary between 100 and 300 rad s^{-1}. This can be explained by the water-bed effect. The surface below one and above one closed by the curve must be equal. Thus, these lower values compensate the higher frequency peak.

The next experiment was carried out in the time domain. Two type of step responses are measured; the reference step response and an input disturbance step response. The

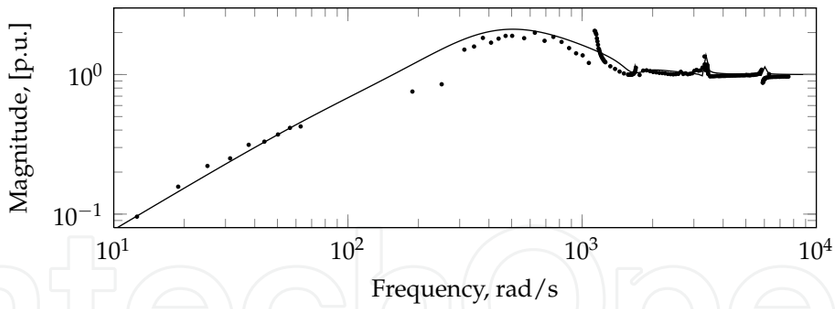

Fig. 9. Output sensitivity function.

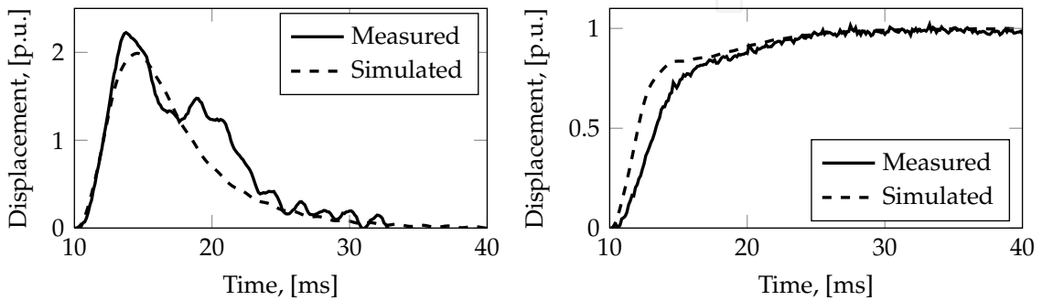

(a) Input disturbance (b) Reference

Fig. 10. Step responses.

results of the measurements are presented in Fig. 10. The reference response shows a good correspondence in the settling time. The disagreement with rise time can be explained by the presented nonlinearities of the system or position of the rotor away from the operational point. Disturbance response shows slightly higher maximum amplitude. Additional oscillations come from the first flexible mode, which is difficult to suppress by the feedback.

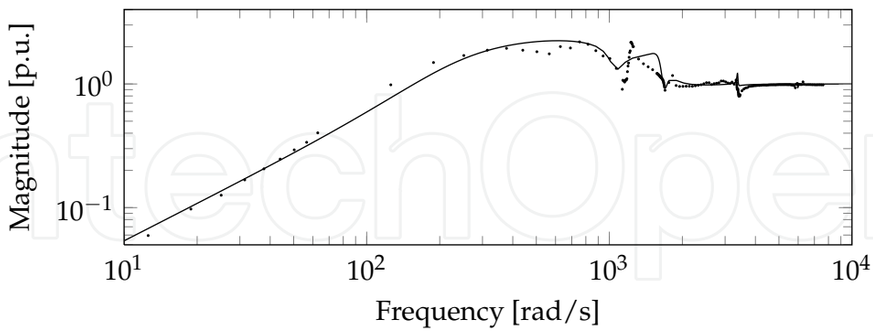

Fig. 11. Output sensitivity function of the H_∞ control.

Similarly, the step responses of the signal-based $\mathcal{H}_\infty$ control (from section 4.2) are presented in Fig. 12. The measured positions for the step responses are filtered by the controller with a relatively low bandwidth of about 110 rad/s. The measured output sensitivity function (Fig. 11) does not differ significantly from the analytical result. The peak unaccounted in the analytically computed values is caused by the structural mode of the base. For the rotational speed in the range from 0 to 6000 rpm the output sensitivity peek varies from 2.618 to 2.625 pu.

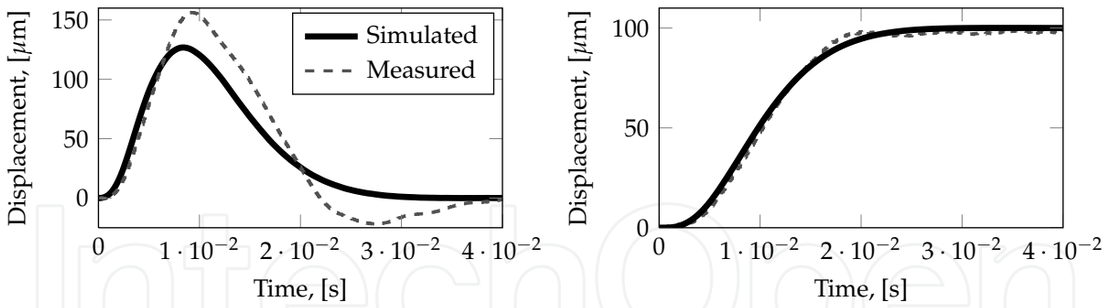

(a) Input disturbance 1 A. (b) Reference 100 μm.

Fig. 12. Step responses of the $\mathcal{H}_\infty$ signal-based design problem.

5. LPV method applied to a gyroscopic AMB rotor system

The rotating speed of the rotor in AMBs is a source of significant uncertainty. What is more important is that it affects the frequency of the flexible modes; these are known to be challenging to suppress with the feedback control (Li, Lin & Allaire, 2006). Especially, the problem is significant for highly gyroscopic systems. The system is considered as a gyroscopic one if a polar moment of inertia is greater than the diametral one $I_\mathrm{p} > I_\mathrm{d}$ or the rotational speed is significant (Schweitzer & Maslen, 2009). A good illustration to the problem is a Campbell diagram presented in Fig. 13.

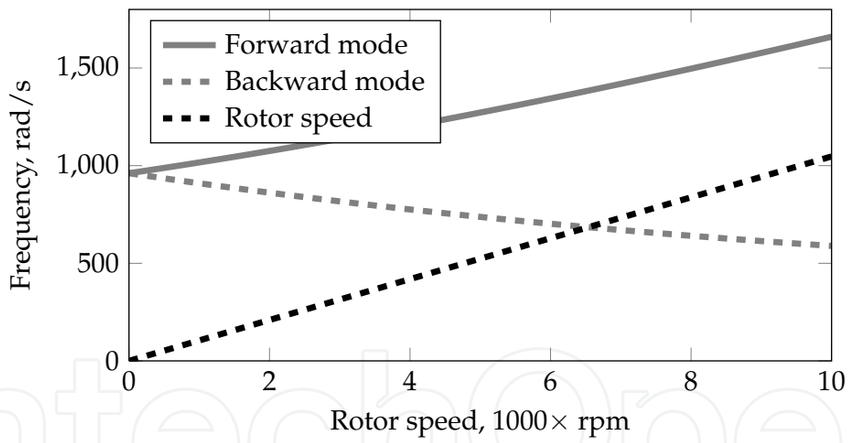

Fig. 13. Campbell diagram.

The significant splitting of the first flexible mode causes the corresponding peak to shift considerably in the frequency response. That affects the controller significantly as it must stabilize the system all the way from the start and up to the nominal speed. The most challenging part of the acceleration curve is around the points where the rotor crosses the flexible mode. In Fig. 13 this happens around 6500 rpm at that point the structural mode gets in resonance with the rotor speed resulting in a significant oscillation magnitude. To overcome this problem, a set of different controllers are synthesized for different rotational speeds. In that case a problem during the switch appears as different controllers have different levels of signals for the same operational point. The problem gets even more significant in MIMO systems. This drawback is treated with bumpless switch techniques (Li (2007); Turner

& Walker (2000)). Another approach to avoid bumps is to interpolate the controllers along with a changing parameter, which is the rotor speed in this case. The last method provides some restrictions, such that interpolated controllers should have the same order and structure. The interpolated controllers are called gain-scheduled controllers (Leith & Leithead, 2000). In particular, the implementation of the AMBs can be presented as a system where the rotor speed is a linear varying parameter. Thus, it is referred to as a category of LPV systems, for which a special LPV gain-scheduling methods can be applied. These methods are free of the above-mentioned drawbacks and provide a unified approach for controller synthesis.

An idea to systematically utilize the rotor speed for the controller adjustment in AMBs was proposed by different authors in different ways. One of the first examples is presented in the work of Matsumura et al. (1996). The authors synthesize a robust loops-shaping controller, which is able to reject sinusoidal disturbance with the rotor rotational frequency. It is carried out by adopting additional boundary constraints for an $\mathcal{H}_\infty$ problem. The model used by the authors contained only rigid modes and the rotor under consideration was without unbalance. Lu et al. (2008) applied an LPV technique for an AMB system. Their model also contained only rigid modes, and additionally, a special technique was used to identify uncertainty and provide weighting functions for the controller synthesis. The authors presented the controller in a set of parameter-dependent LMIs via a Lyapunov function. The basic controller was a general $\mathcal{H}_\infty$ problem with weighting functions.

The problem of LPV controllers was also investigated in the work of Li (2007), where the author compared an LFT approach with a Lyapunov function approach and additionally, with a "frozen" $\mathcal{H}_\infty$ controller. The model used was highly accurate, including not only higher-frequency modes but also structural resonances resulting in a nominal model with as many as 48 states. The author provided the comparison based only on the theoretical γ values of an $\mathcal{H}_\infty$ controllers.

Here, the system model in an LPV form is presented. Based on the Lyapunov function approach to an LPV gain-scheduling a controller synthesis procedure is described. The achieved controllers are compared with the optimal $\mathcal{H}_\infty$ controllers based on the maximum singular values. Additionally, simulations with a non-linear model and unbalance presented in the rotor are discussed. An LPV model of an AMB system is obtained by the same linearization around the operational point as an ordinary AMB model. The system is assumed to be in the operational point in the center of magnetic forces. Only small deviations from that point are considered as a rotor displacement. The rotor movement is translated to the center of mass resulting in a system with five degrees of freedom. The system is decoupled between the z and x, y axes, providing four states for the radial case. The states are displacements in the x and y and rotations around the x and y axes. They are respectively denoted as $\boldsymbol{q}_c^T = [x\ y\ \alpha\ \beta]$. It can be seen that the model (16) and the following (17) has the form of an LPV system

$$\begin{aligned} \dot{\boldsymbol{x}} &= \mathbf{A}(\Omega)\boldsymbol{x} + \mathbf{B}\boldsymbol{u}, \\ \boldsymbol{y} &= \mathbf{C}\boldsymbol{x}. \end{aligned} \tag{31}$$

In general, there are two approaches to the controller synthesis for the LPV plants. The first approach is based on a Lyapunov function. A quadratic Lyapunov function was used to achieve a set of parameter dependent LMIs by Becker & Packard (1994). Later, less conservative results were obtained by incorporating boundaries on parameters variation rates by Wu et al. (1996). As LMIs in this approach are parameter dependent, in general, there are an infinite number of them to solve. Usually, it is suggested to grid the space of varying parameters and achieve a solution for a limited number of points. The method is proposed for

a small number of varying parameters. In an AMB controller synthesis one parameter can be considered as varying. However, the order of the system is rather high and griding with more than five points results in an unrealistically long synthesis time (Li, 2007). Another drawback is that an implementation requires a matrix inversion in real time that is quite challenging with the desired sampling rate on available microcontrollers.
The second one is based on a small gain theorem. The plant is considered as a linear time invariant (LTI) system, which is closed by the feedback loop with a varying parameter. Thus, the full system can be presented as a lower fractional transformation (LFT) of an LTI part and a parameter as presented in Fig. 14(a). Solutions for continuous- and discrete-time cases in a form of LMIs were presented by Apkarian & Gahinet (1995). The solution is conservative compared with the first approach as the realness of parameters is not used. Helmersson (1995) provided an additional research to reduce conservatism by introducing a rate of variation of parameters, which, however, leads to infinite dimensional solvability conditions. A more detailed overview of the research in that field is given by (Leith & Leithead, 2000).
In this work the first approach is taken and in particular, its extension to an affine system proposed by Apkarian et al. (1995). It can be seen from (16) that the system provides a convex set on the speed parameter Ω. Thus, the problem of infinite LMIs is avoided by solving them only at vertexes of the varied parameter. An additional benefit is that the controller implementation is simple and does not require matrix inversion. However, the system considered by Apkarian et al. (1995) neglects the varying state, input, and output transformations, and provides sufficient results under the assumption of a slow-varying parameter as discussed by Leith & Leithead (2000). The slow-varying parameter assumption is valid for an AMB system as the speed variation is relatively slow compared with state variations.

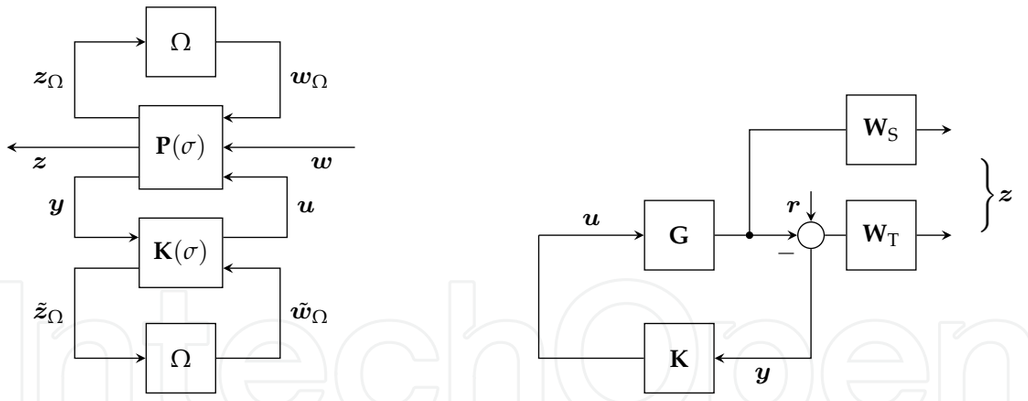

(a) LPV controller structure (b) Mixed sensitivity control problem

Fig. 14. Controller structures.

The general linear $\mathcal{H}_\infty$ problem is to find a controller $\mathbf{K}$ such that it minimizes (26). The generalized plant $\mathbf{P}$ is obtained from the original plant by providing additional exogenous inputs $\boldsymbol{w}$ and outputs $\boldsymbol{z}$ with specified weights to tune the desired system. The particular scheme for the mixed sensitivity problem is presented in Fig. 14(b). The following weights were used to shape the plant to the desired objectives

$$\mathbf{W}_\mathrm{S} = \mathbf{I}_{4\times 4} \cdot 0.5 \frac{s+144}{s+0.144}, \quad \mathbf{W_T} = \mathbf{I}_{4\times 4} \cdot 0.5 \frac{s+0.01}{s+10}. \tag{32}$$

The general rule is that the weight for the sensitivity function is a low-pass filter and for the complementary sensitivity one is a high-pass filter.
Having the generalized plant $\mathbf{P}$ in the form

$$\mathbf{P}(s) = \mathbf{D} + \mathbf{C}(s\mathbf{I} - \mathbf{A})^{-1}\mathbf{B} \tag{33}$$

we follow the authors of (Apkarian et al., 1995) and solve the following LMIs

$$\left(\begin{array}{c|c} \mathcal{N}_\mathrm{R} & 0 \\ \hline 0 & \mathbf{I} \end{array}\right)^T \left(\begin{array}{cc|c} \mathbf{A}_i\mathbf{R} + \mathbf{R}\mathbf{A}_i^T & \mathbf{R}\mathbf{C}_{1i}^T & \mathbf{B}_{1i} \\ \mathbf{C}_{1i}\mathbf{R} & -\gamma\mathbf{I} & \mathbf{D}_{11i} \\ \hline \mathbf{B}_{1i}^T & \mathbf{D}_{11i}^T & -\gamma\mathbf{I} \end{array}\right) \left(\begin{array}{c|c} \mathcal{N}_\mathrm{R} & 0 \\ \hline 0 & \mathbf{I} \end{array}\right) < 0, \quad i = 1, \ldots, r, \tag{34}$$

$$\left(\begin{array}{c|c} \mathcal{N}_\mathrm{S} & 0 \\ \hline 0 & \mathbf{I} \end{array}\right)^T \left(\begin{array}{cc|c} \mathbf{A}_i\mathbf{S} + \mathbf{S}\mathbf{A}_i^T & \mathbf{S}\mathbf{B}_{1i} & \mathbf{C}_{1i}^T \\ \mathbf{B}_{1i}^T\mathbf{S} & -\gamma\mathbf{I} & \mathbf{D}_{11i}^T \\ \hline \mathbf{C}_{1i} & \mathbf{D}_{11i} & -\gamma\mathbf{I} \end{array}\right) \left(\begin{array}{c|c} \mathcal{N}_\mathrm{S} & 0 \\ \hline 0 & \mathbf{I} \end{array}\right) < 0, \quad i = 1, \ldots, r, \tag{35}$$

$$\begin{pmatrix} \mathbf{R} & \mathbf{I} \\ \mathbf{I} & \mathbf{S} \end{pmatrix} \geq 0, \tag{36}$$

where the bases of the null spaces of $(\mathbf{B}_2^T, \mathbf{D}_{12}^T)$ and $(\mathbf{C}_2, \mathbf{D}_{21})$ are denoted $\mathcal{N}_\mathrm{R}$ and $\mathcal{N}_\mathrm{S}$, respectively. Next, the unique solution $\mathbf{X}_\mathrm{cl}$ of the matrix equation $\mathbf{\Pi}_2 = \mathbf{X}_\mathrm{cl}\mathbf{\Pi}_1$ should be computed, where

$$\mathbf{\Pi}_2 = \begin{pmatrix} \mathbf{S} & \mathbf{I} \\ \mathbf{N}^T & \mathbf{0} \end{pmatrix}, \quad \mathbf{\Pi}_1 = \begin{pmatrix} \mathbf{I} & \mathbf{R} \\ \mathbf{0} & \mathbf{M}^T \end{pmatrix} \tag{37}$$

and the matrices $\mathbf{M}$ and $\mathbf{N}$ are such that

$$\mathbf{M}\mathbf{N}^T = \mathbf{I} - \mathbf{R}\mathbf{S}. \tag{38}$$

The controllers for each vertex can be found by solving the following LMI

$$\begin{pmatrix} \mathbf{A}_{\mathrm{K}i}^T\mathbf{X}_\mathrm{cl} + \mathbf{X}_\mathrm{cl}\mathbf{A}_{\mathrm{K}i} & \mathbf{X}_\mathrm{cl}\mathbf{B}_{\mathrm{K}i} & \mathbf{C}_{\mathrm{K}i}^T \\ \mathbf{B}_{\mathrm{K}i}^T\mathbf{X}_\mathrm{cl} & -\gamma\mathbf{I} & \mathbf{D}_{\mathrm{K}i}^T \\ \mathbf{C}_{\mathrm{K}i} & \mathbf{D}_{\mathrm{K}i} & -\gamma\mathbf{I} \end{pmatrix} < 0. \tag{39}$$

Having the state-space matrices for each vertex $\mathbf{A}_{\mathrm{K}i}$, $\mathbf{B}_{\mathrm{K}i}, \mathbf{C}_{\mathrm{K}i}, \mathbf{D}_{\mathrm{K}i}$ the controller for the particular point is obtained as

$$\begin{bmatrix} \mathbf{A}_\mathrm{K}(\Omega) & \mathbf{B}_\mathrm{K}(\Omega) \\ \mathbf{C}_\mathrm{K}(\Omega) & \mathbf{D}_\mathrm{K}(\Omega) \end{bmatrix} = \sum_{i=1}^{r} \alpha_i \begin{bmatrix} \mathbf{A}_{\mathrm{K}i} & \mathbf{B}_{\mathrm{K}i} \\ \mathbf{C}_{\mathrm{K}i} & \mathbf{D}_{\mathrm{K}i} \end{bmatrix}, \tag{40}$$

where α_i is such that

$$\Omega = \left\{ \sum_{i=1}^{r} \alpha_i\omega_i : \ \alpha_i \geq 0, \ \sum_{i=1}^{r} \alpha_i = 1 \right\}. \tag{41}$$

The r denotes the total number of vertices and ω_i the particular vertex. The parameter Ω is measured in real time and the controllers are updated on each step. For the controller testing, we use the system with the Campbell diagram (see Fig. 13) presented above. The polar moment of inertia $I_\mathrm{p} = 10.6\ \mathrm{kg\,m^2}$ is greater than the diametral moment $I_\mathrm{d} = 0.59\ \mathrm{kg\,m^2}$. However, the speed varies from 0 to 10 000 rpm, and thus, the system has significant

gyroscopic effect. The controller is synthesized using the above-mentioned weighting functions (32). As the main objective is the stability of the system, a maximum singular value of sensitivity functions is evaluated. A good starting point for a comparison is an output sensitivity function $\mathbf{S}_o$ (Li, Lin & Allaire, 2006). Additionally, an output complementary sensitivity function $\mathbf{T}_o$ is used for the evaluation.

$$\mathbf{T}_o = \mathbf{GK}\left(\mathbf{I} + \mathbf{GK}\right)^{-1}. \tag{42}$$

The evaluation of the controller is carried out in each point of a variation parameter. It means that the closed loop transfer functions (30) and (42) are calculated at each rotor speed and their peak value is found. The peak values of the MIMO system are defined as maximum singular values in the same fashion as in (26). The achieved results are presented in Fig. 15.

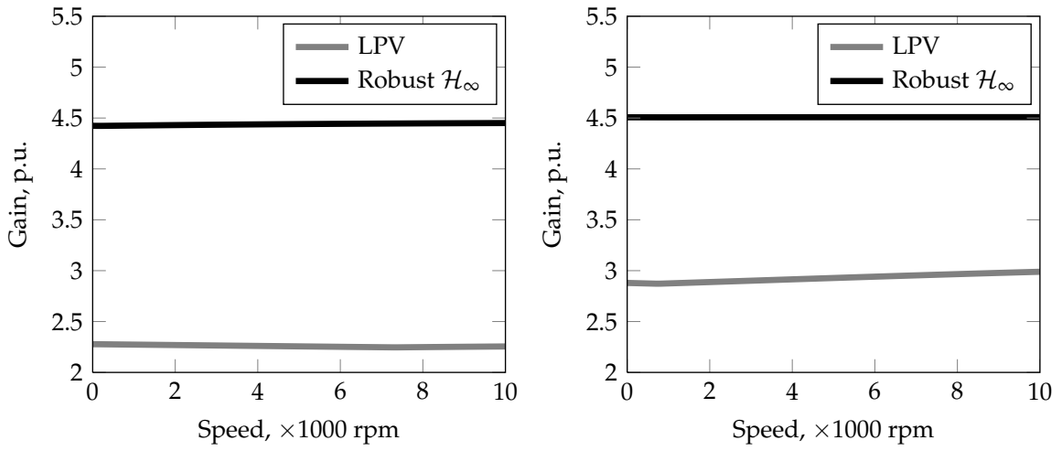

(a) Output sensitivity (b) Output complementary sensitivity

Fig. 15. Maximum values of sensitivity functions.

It is seen that an LPV controller provides a stable system with low values of sensitivity functions. For comparison a robust $\mathcal{H}_\infty$ controller is synthesized using the same weights and the same structure. In this synthesis, speed is treated as a structured uncertainty. In Fig. 15 it is seen that the robust controller has higher peak values and additionally, the values do not change over the parameter variation. The LPV controller peak values are smaller and have some deviation. In general, Fig. 15 shows that the LPV controller provides a greater stability margin.

The previous assessment was based on a theoretical model and provides the basic insight into the stability margins. For a deeper evaluation, simulations with a non-linear model are carried out. The rotor for the simulations is considered to have an imbalance of 0.01 kg, and a system with three flexible modes is used. The force-current relations are non-linear; they include the actuator delay and are based on look-up tables from the switch-reluctance network model.

A typical case of the rotor acceleration is simulated. The speed increases linearly from zero up to the maximum value. The beginning and ending phases of acceleration are smoothed to avoid unrealistic sharp edges. The results are evaluated for an LPV and a robust $\mathcal{H}_\infty$ controllers. The displacements at the A-end in the x direction are presented in Fig. 16.

The LPV controller shows worse performance for the transient response. The magnitude of oscillations is significantly higher around two times. The oscillations take place around the

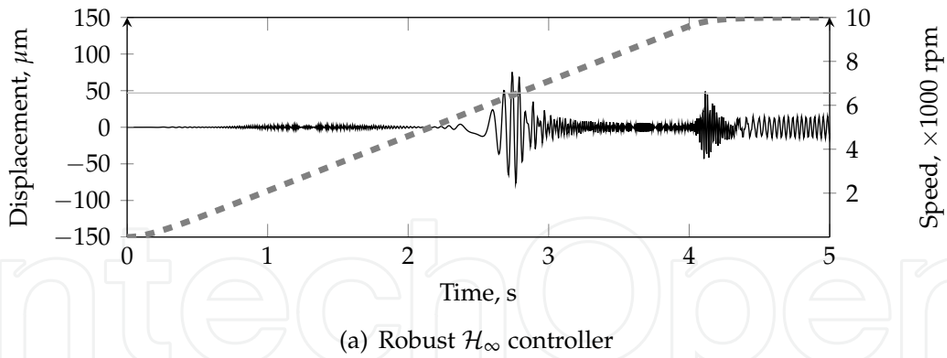

(a) Robust $\mathcal{H}_\infty$ controller

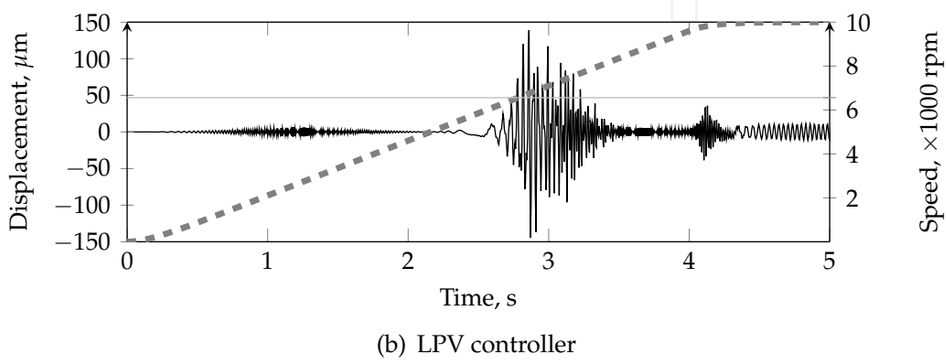

(b) LPV controller

Fig. 16. Rotor acceleration responses.

point of 6500 rpm where the system crosses the first flexible mode. The second point where the system experiences oscillations is close to the maximum speed and it can be explained by the deceleration of the rotor. The LPV controller has a lower magnitude of oscillations around this point; the difference is 35 %. Such a behavior can be explained by an adaptive nature of an LPV controller. In each step, the gains are modified according to the rotational speed. During the acceleration process, the system does not have enough time to adapt. This results in a higher amplitude of oscillations. During the later deceleration phase, the coefficients do not change that fast and performance is better. The speed of the parameter variation is a significant problem for the LPV controllers, and usually the main point of conservatism in that approach (Leith & Leithead, 2000).

The second simulation experiment in the steady state proves that LPV controller provides a better performance. In this experiment, a step disturbance to the x channel of the rotor A-end is applied at the maximum rotational speed. The simulation results are presented in Fig. 17. The magnitude of the disturbance response for an LPV controller is about three times smaller than that of a robust controller. Additionally, the LPV controller does not have coupling between different ends, so the disturbance does not propagate through the system.

6. Real-time operating conditions

The AMB-based system requires hard-real time controllers. In the case of a robust control strategy, the control law is of higher complexity than other solutions. Therefore, the implementation of the control law must fulfill the requirements of the target control system such as finite precision of the arithmetic and number format and available computational

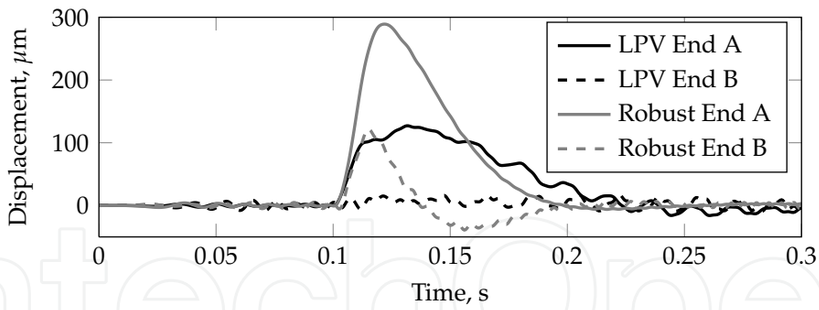

Fig. 17. Step disturbance response for controllers in the x direction.

power. The digital control realization requires a digital controller that matches the continuous form in the operating frequency range. The controllers for the radial suspension of the AMB rotor system are tested using a dSpace DS1005-09 digital control board and a DS4003 Digital Input/Output system board as a regulation platform. The Simulink and Real-time Workshop software are applied for automatic program code generation. The selected sampling rate is 10 kHz. The resolution of the applied ADCs is 16 bits. The control setup limits the maximum number of states of the implemented controllers to 28 states.

7. Conclusions

The chapter discusses options and feasible control solutions when building uncertain AMB rotor models and when designing a robust control for the AMB rotor systems. The review of the AMB systems is presented. The recommendations for difficult weight selection in different weighting schemes are given. Design-specific problems and trade-offs for each controller are discussed. It is shown that the operating conditions of the selected real-time controllers satisfy the control quality requirements. The resulting order of the controller depends on the complexity of the applied weighting scheme, plant order, and applied uncertainties. The detailed interconnections lead to controllers, which are difficult to implement and are not transparent. However, the too simple weighting schemes cannot provide sufficient design flexibility with respect to the multi-objective specification. For the systems with considerably gyroscopic rotors and high rotational speeds, the LPV method provides a significantly better solution than nonadaptive robust control methods.

8. Acknowledgement

This chapter was partially founded by AGH Research Grant no 11.11.120.768

9. References

Apkarian, P. & Gahinet, P. (1995). A convex characterization of gain-scheduled H_∞ controllers, *Automatic Control, IEEE Transactions on* 40(5): 853–864.

Apkarian, P., Gahinet, P. & Becker, G. (1995). Self-scheduled H_∞ control of linear parameter-varying systems: a design example, *Automatica* 31(9): 1251–1261.

Battachatyya, S. P., Chapellat, H. & Keel, L. H. (1995). *Robust Control The Parametric Approach*, Prentice Hall.

Becker, G. & Packard, A. (1994). Robust performance of linear parametrically varying systems using parametrically-dependent linear feedback, *Systems & Control Letters* 23(3): 205–215.

Fujita, M., Hatake, K. & Matsumura, F. (1993). Loop shaping based robust control of a magnetic bearing, *Control Systems Magazine, IEEE* 13(4): 57–65.

Fujita, M., Namerikawa, T., Matsamura, F. & Uchida, K. (1995). mi-synthesis of an electromagnetic suspension system, *IEEE Transactions on Automatic Control* 40: 530–536.

Glover, K. & McFarlane, D. (1989). Robust stabilization of normalized coprime factor plant descriptions with H_∞-bounded uncertainty, *Automatic Control, IEEE Transactions on* 34(8): 821–830.

Gosiewski, Z. & Mystkowski, A. (2008). Robust control of active magnetic suspension: Analytical and experimental results, *Mechanical Systems and Signal Processing* 22: 1297–1303.

Gu, D., Petkov, P. & Konstantinov, M. (2005a). *Robust Control Design with MATLAB*, Springer.

Gu, D.-W., Petkov, P. & Konstantinov, M. (2005b). *Robust Control Design with MATLAB*, Springer, Leipzig, Germany.

Helmersson, A. (1995). *Methods for robust gains scheduling*, PhD thesis, Linkoping University.

InTeCo (2008). *MLS2EM, Magnetic Levitation User's Guide*, InTeCo, Poland.

Jastrzebski, R. (2007). *Design and Implementation of FPGA-based LQ Control of Active Magnetic Bearings*, PhD thesis, LUT, Finland.

Jastrzebski, R., Hynynen, K. & Smirnov, A. (2010). *H*-infinity control of active magnetic suspension, *Mechanical Systems and Signal Processing* 24(4): 995–1006.

Jastrzebski, R. & Pöllänen, R. (2009). Centralized optimal position control for active magnetic bearings - comparison with decentralized control, *Electrical Engineering* 91(2): 101–114.

Kwakernaak, H. (1993). Robust control and hinf-optimization tutorial paper, *Automatica* 29: 253–273.

Kwakernaak, H. (2002). H2-optimization theory and applications to robust control design, *Annual Reviews in Control* 26: 45–56.

Lanzon, A. & Tsiotras, P. (2005). A combined application of H infin; loop shaping and mu;-synthesis to control high-speed flywheels, *Control Systems Technology, IEEE Transactions on* 13(5): 766–777.

Leith, D. J. & Leithead, W. E. (2000). Survey of gain-scheduling analysis and design, *International Journal of Control* 73(11): 1001–1025.

Li, G. (2007). *Robust stabilization of rotor-active magnetic bearing systems*, PhD thesis, University of Virginia.

Li, G., Lin, Z. & Allaire, P. (2006). Uncertainty classification of rotor-amb systems, *Proc. of* 11th *International Symposium on Magnetic Bearings*.

Li, G., Lin, Z., Allaire, P. & Luo, J. (2006). Modeling of a high speed rotor test rig with active magnetic bearings, *Journal of Vibration and Acoustics* 128: 269–281.

Limebeer, D. J. N., Kasenally, E. M. & Perkins, J. D. (1993). On the design of robust two degree of freedom controllers, *Automatica* 29(1): 157–168.

Losch, F. (2002). *Identification and Automated Controller Design for Active Magnetic Bearing Systems*, Swiss Federal Institute of Technology, ETH Zurich.

Lu, B., Choi, H., Buckner, G. D. & Tammi, K. (2008). Linear parameter-varying techniques for control of a magnetic bearing system, *Control Engineering Practice* 16(10): 1161–1172.

Lunz, J. (1989). *Robust Multivariable Feedback Control*, Prentice Hall, London.

Matsumura, F., Namerikawa, T., Hagiwara, K. & Fujita, M. (1996). Application of gain scheduled H_∞ robust controllers to a magnetic bearing, *Control Systems Technology, IEEE Transactions on* 4(5): 484–493.

Moser, A. (1993). Designing controllers for flexible structures with H-infinity/μ-synthesis, *IEEE Control Systems* pp. 79–89.

Mystkowski, A. & Gosiewski, Z. (2009). Uncertainty modeling in robust control of active magnetic suspension, *Solid State Phenomena* 144: 22–26.

Oliveira, V., Tognetti, E. & Siqueira, D. (2006). Robust controllers enhanced with design and implementation processes, *IEEE Trans. on Education* 49(3): 370–382.

Pilat, A. (2002). *Control of Magnetic Levitation Systems*, PhD thesis, AGH University of Science and Technology.

Pilat, A. (2009). Stiffness and damping analysis for pole placement method applied to active magnetic suspension (in polish), *Automatyka* 13: 43–54.

Pilat, A. (2010). mi-synthesis of robust controller for active magnetic levitation system, *MSM 2010 : Mechatronic Systems and Materials : 6th international conference : 5-8 July, Opole, Poland*.

Pilat, A. & Piatek, P. (2008). Multichannel control and measurement board with parallel data processing (in polish), *in* L. Trybus & S. Samolej (eds), *Recent advances in control and automation*, Academic Publishing House EXIT, pp. 00–00.

Pilat, A. & Turnau, A. (2005). Self-organizing fuzzy controller for magnetic levitation system, *Computer Methods and Systems, Krakï£¡w, Poland*, pp. 101–106.

Pilat, A. & Turnau, A. (2009). Neural adapted controller learned on-line in real-time, *14 International Conference on Methods and Models in Automation and Robotics, 19-21 August, Miedzyzdroje, Poland*.

Safonov, M. G. & Chiang, R. Y. (1988). A Schur Method for Balanced Model Reduction, *American Control Conference, 1988*, pp. 1036–1040.

Sawicki, J. & Maslen, E. (2008). Toward automated amb controller tuning: Progress in identification and synthesis, *Proc. of* 11$^{\text{th}}$ *International Symposium on Magnetic Bearings*, pp. 68–74.

Scherer, C., Gahinet, P. & Chilali, M. (1997). Multiobjective output-feedback control via LMI optimization, *IEEE Transations on Automatic Control* 42(7): 896–911.

Schweitzer, G. & Maslen, E. (2009). *Magnetic Bearings: Theory, Design, and Application to Rotating Machinery*, Springer, New York.

Sefton, J. & Glover, K. (1990). Pole/zero cancellations in the general [infinity] problem with reference to a two block design, *Systems and Control Letters* 14(4): 295–306.

Skogestad, S. & Postlethwaite, I. (2005). *Multivariable Feedback Control Analysis and Design*, 2 edn, John Wiley & Sons Ltd., England.

Turner, M. C. & Walker, D. J. (2000). Linear quadratic bumpless transfer, *Automatica* 36(8): 1089–1101.

Whidborne, J., Postlethwaite, I. & Gu, D.-W. (1994). Robust controller design using H_∞ loop-shaping and the method of inequalities, *IEEE Transations on Control Systems Technology* 2(2): 455–461.

Wu, F., Yang, X. H., Packard, A. & Becker, G. (1996). Induced L2-norm control for LPV systems with bounded parameter variation rates, *International Journal of Robust and Nonlinear Control* 6(9-10): 983–998.

Zhou, K. (1998). *Essentials of Robust Control*, Prentice-Hall, Upper Saddle River, NJ.

Zhou, K., Doyle, J. & Glover, K. (1996). *Robust and Optimal Control*, Prentice-Hall, Englewood Cliffs, NJ.

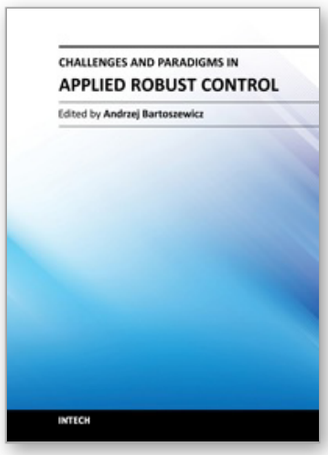

Challenges and Paradigms in Applied Robust Control

Edited by Prof. Andrzej Bartoszewicz

ISBN 978-953-307-338-5
Hard cover, 460 pages
Publisher InTech
Published online 16, November, 2011
Published in print edition November, 2011

The main objective of this book is to present important challenges and paradigms in the field of applied robust control design and implementation. Book contains a broad range of well worked out, recent application studies which include but are not limited to H-infinity, sliding mode, robust PID and fault tolerant based control systems. The contributions enrich the current state of the art, and encourage new applications of robust control techniques in various engineering and non-engineering systems.

How to reference

In order to correctly reference this scholarly work, feel free to copy and paste the following:

Rafal P. Jastrzebski, Alexander Smirnov, Olli Pyrhönen and Adam K. Piłat (2011). Discussion on Robust Control Applied to Active Magnetic Bearing Rotor System, Challenges and Paradigms in Applied Robust Control, Prof. Andrzej Bartoszewicz (Ed.), ISBN: 978-953-307-338-5, InTech, Available from: http://www.intechopen.com/books/challenges-and-paradigms-in-applied-robust-control/discussion-on-robust-control-applied-to-active-magnetic-bearing-rotor-system

INTECH
open science | open minds

InTech Europe
University Campus STeP Ri
Slavka Krautzeka 83/A
51000 Rijeka, Croatia
Phone: +385 (51) 770 447
Fax: +385 (51) 686 166
www.intechopen.com

InTech China
Unit 405, Office Block, Hotel Equatorial Shanghai
No.65, Yan An Road (West), Shanghai, 200040, China
中国上海市延安西路65号上海国际贵都大饭店办公楼405单元
Phone: +86-21-62489820
Fax: +86-21-62489821

IntechOpen